Endocavity Ultrasound Probe Manipulators

Dan Stoianovici, Chunwoo Kim, *Student Member, IEEE*, Felix Schäfer, Chien-Ming Huang, Yihe Zuo, Doru Petrisor, and Misop Han

***Abstract*—We developed two similar structure manipulators for medical endocavity ultrasound probes with 3 and 4 degrees of freedom (DoF). These robots allow scanning with ultrasound for 3-D imaging and enable robot-assisted image-guided procedures. Both robots use remote center of motion kinematics, characteristic of medical robots. The 4-DoF robot provides unrestricted manipulation of the endocavity probe. With the 3-DoF robot the insertion motion of the probe must be adjusted manually, but the device is simpler and may also be used to manipulate external-body probes. The robots enabled a novel surgical approach of using intraoperative image-based navigation during robot-assisted laparoscopic prostatectomy (RALP), performed with concurrent use of two robotic systems (Tandem, T-RALP). Thus far, a clinical trial for evaluation of safety and feasibility has been performed successfully on 46 patients. This paper describes the architecture and design of the robots, the two prototypes, control features related to safety, preclinical experiments, and the T-RALP procedure.**

***Index Terms*—Image guide, medical robot, prostatectomy, remote center of motion (RCM), transrectal ultrasound (TRUS) probe, ultrasound.**

I. Introduction

ULTRASOUND is a commonly used medical imaging modality. Its nonionizing radiation and near real-time display make ultrasound a preferred modality for most image-guided procedures and interventions. Basic ultrasound generates two-dimensional (2-D) images depicting a cross-sectional view of the anatomy. The ultrasound probes (piezoelectric transceivers) are typically operated manually. Trained operators gain mnemonic 3-D perception of the anatomy by moving the probe. However, the position of the probe is not typically recorded with freehand motion, deterring further 3-D image processing. But if a robot manipulates the probe, the coordinate frames of the acquired images are readily available. As such, typical 2-D probes can be used for 3-D ultrasound scanning. Then, based on the images, the robot may automatically position the probe to image a certain site and/or assist with image-guided interventions (IGI) such as needle biopsy.

Manuscript received September 6, 2011; revised February 13, 2012; accepted March 27, 2012. Date of publication May 3, 2012; date of current version January 18, 2013. Recommended by Technical Editor A. Menciassi. This work was supported in part by the National Cancer Institute under Award CA141835, in part by the Sidney Kimmel Comprehensive Cancer Center, Johns Hopkins, and in part by Hitachi-Aloka Medical Ltd.

The authors are with the Urology Robotics Laboratory, School of Medicine, The Johns Hopkins University, Baltimore, MD 21224 USA (e-mail: dss@jhu.edu; cwkim@jhu.edu; doru@jhu.edu; misop@jhmi.edu; schaefer@dimec.unige.it; snoopy67@ms19.hinet.net; zuoyihe19841228@gmail.com).

Color versions of one or more of the figures in this paper are available online at http://ieeexplore.ieee.org.

Digital Object Identifier 10.1109/TMECH.2012.2195325

3-D ultrasonography is not a novel concept. Indeed, several commercial 3-D ultrasound probes and equipment are available. These offer imaging advantages but remain difficult to use freehanded in IGI.

Ultrasound probe trackers are now emerging to assist in IGIs. For this, probes are instrumented with optical or magnetic position sensors [1], or passive encoded positioning arms [2]. An advantage of the arms is that they can be locked to support the probe in place. Furthermore, robotic arms may also execute actuated scanning and targeting.

A Mitsubishi PA-10 industrial robot was initially used to manipulate an ultrasound [3]. The medical environment, however, has special requirements demanding purpose-built devices [4]. Perhaps, the first medical ultrasound robot was developed in the late 1990s at the University of British Columbia, Canada [5]. This robot supported an external-body-type ultrasound probe with 6 degrees of freedom (DoF) and had numerous features that set it ahead of its time, including one the very first synergistic, man–machine interaction systems.

Very few purpose built ultrasound manipulators were developed since. In 2004, the OTELO system was reported from the University of Orleans, France, for tele-echography [6], [7]. This was also a 6-DoF manipulator for an external-body probe, but used different kinematics and was more compact. Most recently, a parallel-link ultrasound manipulator has been built at Tokyo University, Japan, also with 6 DoF and for external-body probes [8]. One of its novelties is the gravity-balanced structure that helps the sonographer to operate the probe weightlessly.

At the other end of the DoF range are systems made for specific clinical procedures that integrate ultrasound probes. These typically implement only 1 or 2 active DoF for probe manipulation, being supplemented by prepositioning arms with passive degrees of adjustment (DoA). For example, in 2009 two ultrasound-guided needle robots were reported, from Singapore [9] and Canada [10]. Both systems were for transperineal needle access of the prostate for biopsy and brachytherapy, respectively. These include novel high-DoF mechanisms for needle handling but only 1 DoF for either insertion or probe spinning, respectively. A 2-DoF endocavity probe manipulator actuating both the insertion and spin motions has been recently reported by the University of British Columbia group, including vibrations for inducing ultrasound elastography [11]. Most recently, a system has been developed for breast biopsy including a manipulator for a special breast ultrasound probe [12].

Overall, few ultrasound robots have been developed to date with either 1–2 DoF or full 6-DoF maneuverability. Our developments fall in the middle DoF range. This fills a gap of technology for endocavity ultrasound.

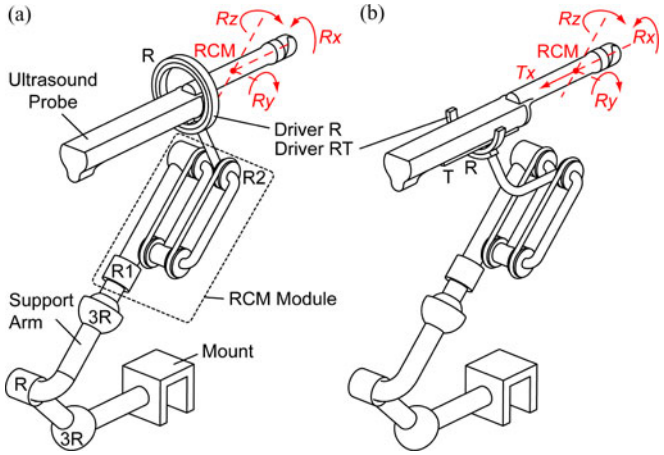

Fig. 1. Kinematic diagram of the robots: (a) 3 DoF with R driver and (b) 4 DoF with RT driver.

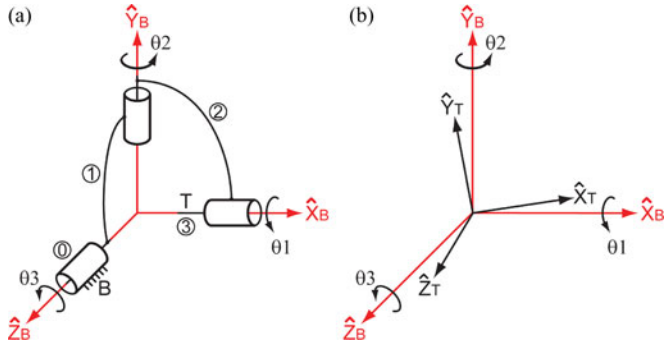

Fig. 2. (a) Symbolic representation of the RCM3 mechanism implementing *Z–Y–X* Euler angles and (b) Fixed frame *X–Y–Z* rotations of its tool frame {T} in the fixed base frame {B}.

We report the development of two similar structure robots (3 DoF and 4 DoF) to support and manipulate endocavity ultrasound probes for image scanning and subsequent image-guided navigation and interventions. Both robots have been used clinically. Kinematics, design, and safety aspects are presented in this paper along with the descriptions of some preclinical experiments and a first clinical trial.

II. Kinematic Structure

The robots include remote center of motion (RCM) mechanisms, characteristic of medical robots [4], [13]–[16]. The RCM mechanism allows a medical instrument to pivot about a fulcrum point that is located remotely from the mechanism. This pivoting motion is common for passing medical instruments through a minimally invasive entry port or natural orifice, typically placing the RCM fulcrum near the entry. Operating the instrument about the entry port also includes instrument insertion and spin, for a total of 4 DoF. This restricted "keyhole" manipulation is also common for operating endocavity ultrasound probes.

The mechanical structure of the robot comprises a mount, a passive support arm, an RCM orientation module, and a driver to support the ultrasound probe, as shown in Fig. 2. The mount attaches to a fixed base such as an operative table. The passive support arm presents 7-DoA with two spherical joints (3R) and one cylindrical joint (R) which can be locked in place to support the device as needed.

The RCM module presents two rotary DoF (R_z, R_y) with axes intersecting at the RCM point. Our RCM module uses a parallelogram mechanism implemented with two belts [17]–[19] and is driven by custom ball-worm transmissions [20], [21].

The ultrasound driver is attached to the RCM module. Two versions of the driver have been developed, with 1 DoF [Driver R, Fig. 1(a)] and 2 DoF [Driver RT, Fig. 1(b)]. Both versions implement a rotary DoF (R_x) with the axis passing through the RCM point. In addition to the other two rotations of the RCM module, these give full orientation capabilities about the fulcrum point. The RT driver includes an additional DoF for instrument translation (T_x) along the same axis.

The RCM module and the ultrasound driver implement an RCM mechanism with 3 DoF (RCM3). The orientation of the tool frame T (ultrasound probe) may be described by a classic set of yaw, pitch, and roll Euler angles (*Z–Y–X*).

The RCM3 manipulator is symbolically represented in Fig. 1, at a position where its axes are orthogonal. Since the belt mechanism of the RCM module couples the motion of its joints for the remote axis (R_y), all parallelogram joints are represented by a single joint connecting links 1 and 2. Therefore, RCM3 implements a sequence of three rotations ($\theta_3, \theta_2, \theta_1$) performed about the axes of the moving frames, starting at the base frame {B} of link 0 to the tool frame {T} of link 3.

The link configuration chosen has simplicity advantages, as follows. The Euler $\widehat{Z} \rightarrow \widehat{Y} \rightarrow \widehat{X}$ rotation about the axes of the moving frames of the manipulator [see (Fig. 2(a)] can be expressed as

$$ {}^{B}_{T}R = {}^{0}_{3}R = {}^{0}_{1}R\ {}^{1}_{2}R\ {}^{2}_{3}R = R_z(\theta_3)\, R_y(\theta_2)\, R_x(\theta_1) \qquad (1) $$

where R denotes rotation matrices of the individual frames associated with the links. Alternatively, if the tool frame orientation is expressed as a sequence of rotations about the $\widehat{X}_B \rightarrow \widehat{Y}_B \rightarrow \widehat{Z}_B$ axes of the fixed {B} coordinate frame shown in Fig. 2(b), these three fixed frame sequential rotations move an arbitrary point ${}^{B}P$ defined in the base frame {B} as follows:

$$ \begin{array}{lrr} \theta_1: & {}^{B}P \rightarrow & R_x(\theta_1)\, {}^{B}_{P} \\ \theta_2: & R_x(\theta_1)\, {}^{B}P \rightarrow & R_y(\theta_2)\, R_x(\theta_1)\, {}^{B}_{P} \\ \theta_3: & R_y(\theta_2)\, R_x(\theta_1)\, {}^{B}P \rightarrow & R_z(\theta_3)\, R_y(\theta_2)\, R_x(\theta_1)\, {}^{B}_{P} \end{array} \qquad (2) $$

so that the overall rotation is

$$ R_{xyz} = R_z(\theta_3)\, R_y(\theta_2)\, R_x(\theta_1). \qquad (3) $$

Since individual axis rotation matrices R_x, R_y, R_z in (1) and (3) are the same, it results that ${}^{B}_{T}R = R_{xyz}$. As usual, this confirms that fixed *X–Y–Z* rotations and Euler *Z–Y–X* yield the same final orientation. For the reported RCM3 mechanism, this means that the direct and inverse kinematic solutions are trivial: RCM3 joint angles θ_1, θ_2, θ_3 are equal to their respective tool frame angles θ_1, θ_2, θ_3 measured about the base coordinate system, and vice versa.

When the tool frame orientation is parameterized by other means, these can easily be derived in a closed form. For example, from (1) the direct kinematic solution to a tool frame described by a rotation matrix is

$$
{}^{B}_{T}R = \begin{bmatrix} c3 & -s3 & 0 \\ s3 & c3 & 0 \\ 0 & 0 & 1 \end{bmatrix} \begin{bmatrix} c2 & 0 & s2 \\ 0 & 1 & 0 \\ -s2 & 0 & c2 \end{bmatrix} \begin{bmatrix} 1 & 0 & 0 \\ 0 & c1 & -s1 \\ 0 & s1 & c1 \end{bmatrix}
$$
$$
= \begin{bmatrix} c2c3 & s1s2c3 - c1s3 & c1s2c3 + s1s3 \\ c2s3 & s1s2s3 + c1c3 & c1s2s3 - s1c3 \\ -s2 & s1c2 & c1c2 \end{bmatrix} \tag{4}
$$

where $sn = \sin\theta_n$ and $cn = \cos\theta_n$, for $n = 1, 2, 3$.

For the inverse kinematic, if the elements r of the tool frame rotation matrix are

$$
{}^{B}_{T}R = \begin{bmatrix} r_{11} & r_{12} & r_{13} \\ r_{21} & r_{22} & r_{23} \\ r_{31} & r_{32} & r_{33} \end{bmatrix} \tag{5}
$$

the RCM joint angles are then derived as usual, observing that $r_{11}^2 + r_{21}^2 = c2^2$. When $c2 \neq 0$

$$
\begin{aligned}
\theta_2 &= \tan^{-1} \frac{-r_{31}}{\sqrt{r_{11}^2 + r_{21}^2}} \\
\theta_3 &= \tan^{-1} \frac{r_{21}}{r_{11}} \\
\theta_1 &= \tan^{-1} \frac{r_{32}}{r_{33}}.
\end{aligned} \tag{6}
$$

These also point out the singularity of the RCM3 mechanism for $\theta_2 = \pm 90^\circ$. The RCM3 mechanism loses a degree of freedom when its $\widehat{X}$ and $\widehat{Z}$ axes are aligned. These positions are avoided by hardware and software limits and offsetting this angle by design, as shown next.

III. Manipulator Design

The structures of the 3- and 4-DoF manipulators are presented in Fig. 3. The RCM module is represented in its folded position (the parallelogram it describes is collapsed). Achieving this folded position has been a novelty of our belt-drive RCM mechanism [18], [19], [21], and its advantage is a much more compact structure than classic bar-type RCMs which cannot be folded [13].

As shown in Fig. 3, the R and RT drivers are designed to mount with θ_2^0 angle offsets, chosen to increase the clearance of the mechanism with respect to the patient. Moreover, the RT Driver was designed to mount on the opposite side of the RCM module, thus reducing their interference.

Driver R: An exploded view of the driver R assembly components is presented in Fig. 4. The ultrasound probe is supported with an adapter that allows its consistent repetitive mounting. A linear scale (ruler) and a manual adjustment knob are included to set the depth of the probe as needed (1-DoA).

The driver presents a disk-like structure. The adapter is connected to a central rotor, supported by a set of bearings. To reduce size, the bearings are custom made so that their races are built within the body and cap of the driver. Instead of the cage bearings, a sequence of intercalated slightly smaller balls

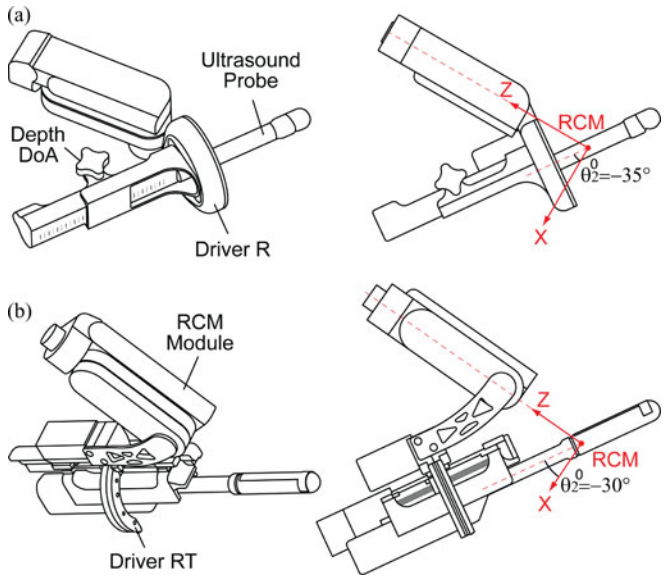

Fig. 3. Ultrasound robots with (a) 3 DoF and (b) 4 DoF.

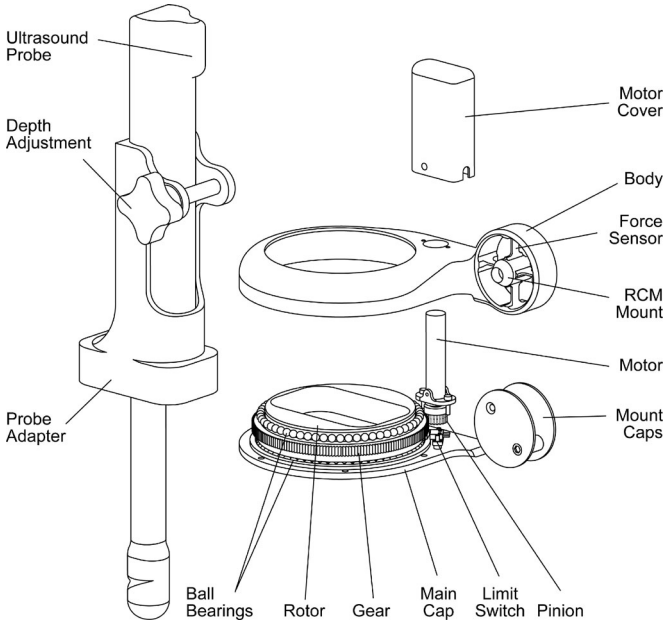

Fig. 4. Ultrasound driver R: exploded view.

are used (Φ4 mm Torlon main balls and Φ5/32″ = 3.969 mm PTFE "cage" balls). These normally roll in a reversed direction than the main balls possibly reducing friction. The rotor is engaged by a spur gear transmission (FFD105-180 gear and PFS80-22 pinion, WM Berg, Cudahy, WI) from a geared servomotor (Series RE10, 12 V, 1.5 W, 256:1 transmission ratio, 0.15 Nm planetary gearhead, 12 count magnetic encoder, Part #305248, Maxon Motor, Sachseln, Switzerland). A limit switch (subminiature series, D2MQ, Omron, Kyoto, Japan) mounted on the base triggers a rotary location (rideover) for homing the incremental encoder.

The body of the driver is connected to the RCM module through a custom-made sensor to measure the force exerted on

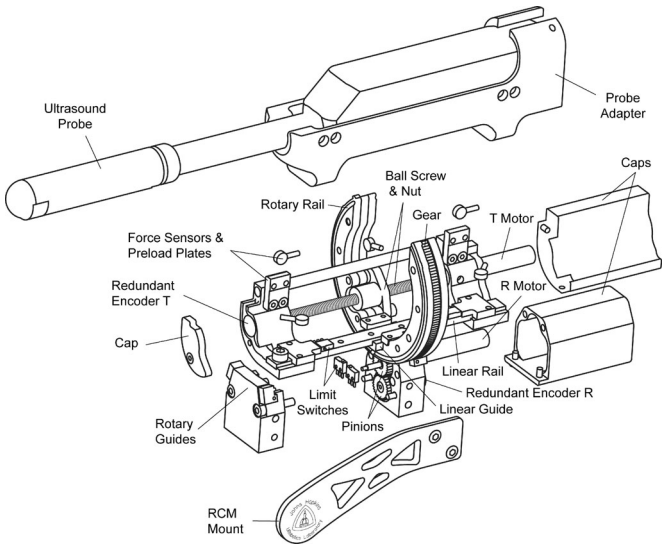

Fig. 5. Ultrasound driver RT: exploded view.

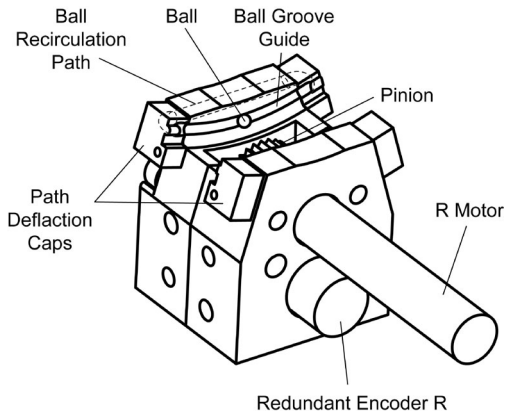

Fig. 6. Ball circulation path within the rotary guide.

the probe in its axial direction. Strain concentration elements were built and strain gauges (1-LY13-3/120, HBM, Darmstadt, Germany) were applied to the opposite sides of the elements. The sensor was calibrated experimentally.

Driver RT: Fig. 5 shows an exploded view of the RT driver. A probe is mounted with an adapter so that it is coaxial with the rotary axis of the driver. The adapter is attached to the driver through preload plates of four force sensors. These are supported by a linear rail and guide (miniature series, 10 mm width, 9706K51, respectively, 9706K1, McMaster Carr, Chicago, IL). The rail is actuated with a ball screw (miniature metric series, ϕ6 mm, 1 mm pitch, McMaster 6638K1) by a geared servomotor (series RE10, 12 V, 1.5 W, gear ratio 16:1, 16 count/rev. magnetic encoder, Part #273200, Maxon Motor). The guide block is then supported by the rail structure of a custom-built rotary rail and guide. This presents a horseshoe profile and includes a spur gear sector (WM Berg FFD105-186, with 186 teeth). The rotary rail and guide are built similar to linear ball rails, but are circular. Two series of steel balls ($3/32'' = 2.381$ mm diameter) circulate in grooves made on each side of the rail, and recirculate through special paths made within the guides, as shown in Fig. 6 (guide only shown).

Actuation of the horseshoe-shaped rotary rail is given by its gear sector engaged by a pinion (WM Berg PFS80-28, with 28 teeth) from a geared servomotor (series RE10, 12 V, 1.5 W, 256:1 0.15 Nm gear head, 12 count/rev. magnetic encoder, Part #305248, Maxon Motor). Both axes are equipped with redundant encoders (3725, RE 12D300-201-1, 300 count/rev., Copal Electronics, Tokyo, Japan): one connected directly to the screw and the other to the pinion of the rotary axes through another pinion (WM Berg PFS80-28). A set of hardware limit switches (subminiature series, D2MQ, Omron, Kyoto, Japan) is used on each axis. Since both the motor and redundant encoders are incremental, one per axis is also used for homing.

A set of five force sensors are used to measure all force–torque interactions of the probe, except for the torque exerted about its longitudinal axis. All are miniature quartz sensor series with extremely flat design for measuring quasi-static forces (SlimLine Sensor 9131B21, 0–2500 N, $\phi 7 \times 3$ mm, Kistler Group, Winterthur, Switzerland). Four of the sensors are intercalated between the probe adapter and the RT Driver, to measure all forces and moments exerted lateral to the probe. The axial force is measured by a sensor intercalated between the ball nut and the rotary rail.

The horseshoe shape was chosen to clear the space above the ultrasound probe for needle access. The arrangement and order of the R and T guides and rails presented above have been chosen 1) to ensure that the space cleared for access remains above the probe during rotation and 2) to render a compact and sturdy mechanical structure. Since the probe adapter must have a long shape to firmly hold the handle of the slender-shaped probe, the most appropriate place for the linear rail resides along its side. The linear guide must then attach to the horseshoe rotary rail. Consequently, the rotary guide must have based the driver.

IV. Robot Prototypes

Both the R and RT driver robots have been built, consecutively (see Fig. 7). The 4-DoF robot uses an updated RCM module. Both versions have a compact structure and, due to their RCM kinematic architecture, have a wide range of motion which enables typical positioning and scanning motion similar to human maneuverability (see Table I). The table also shows the offsets θ_2^0 to the folded/collapsed position of the RCM module. Inclusive software limits are imposed to avoid mechanical interference of the driver and RCM modules. Together with the offsets, these clear near singularity positions (6). Further inclusive software limits are then set for safety, as needed clinically.

V. Motion Control, Safety Features, and Image Processing

The control hardware is similar for the two robots. For the 4 DoF, the controller of the robot is based on an Intel (Santa Clara, CA), Intel Core i7-960 processor on Asus (ASUSTeK Computer, Inc., Taiwan), P6$\times$58D motherboard with 4 GB of

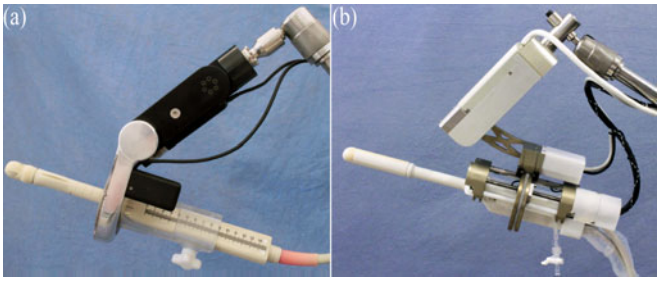

Fig. 7. (a) 3-DoF and (b) 4-DoF ultrasound robots.

TABLE I
AXES LIMITS AND OFFSETS

Driver	Rx[°]	Ry [°]		Ry [°]	Tx
	θ_1	Folded RCM Offset θ_2^0	Hardware θ_2	θ_3 [°]	[mm]
R	±∞	-35°	-53° to 135°	±∞	N/A
RT	±115°	-30°	-49° to 60°	±90°	±35

DDR3 memory running Windows 7, 32-bit operating system (Microsoft Corporation, Redmond, WA). This is equipped with a built-in uninterruptable power supply (ECO750UPS, Tripp Lite, Chicago, IL) for safety and short-range transportability in a robot-ready state. Motor control is implemented on an MC8000-DUAL (PMDI, Victoria, BC, Canada) motion control card with onboard digital signal processor for real-time motion control. This card has dual quadrature decoders and counters for each axis for the motor and redundant encoders of each axis. Linear servomotor amplifiers Maxon 250521, LSC 30/2 30 V/2 A are used for all four axes. A purpose-built relay and watchdog board is included. A single 50-wire cable connects the PC to a connection box at the base of the passive arm. The connection box also includes the amplifiers for force sensors to reduce the length of the sensor cables.

The watchdog checks the state of several components of the system once every 100 ms, disabling power to the motor amplifiers if a faulty condition is detected. Visual signs are used to signal the operation state of the robot. An emergency stop button disables the system and also suspends motor amplifier power. The operation of the system is performed from either a 2-DoF joystick equipped with RCM or RT driver enabled buttons, or under numeric control. For the R-driver version, the translation joystick axis remains unused.

The control software consists of axis-level motion control components, robot kinematics software, ultrasound visualization, and 3-D image processing software. Motion control software is built in Visual C++ (Microsoft Corporation, Redmond, WA) based on high-level libraries of the motion control card (MCI-SoftLib, PMDI).

Imaging components and interface to the robot are also written in Visual C++ based on the Amira Visualization platform (Visage Imaging, Inc., San Diego, CA). When a probe is manipulated by a robot, the space swept by the images may be rendered volumetrically. 3-D image reconstructions from 2-D images require the position and orientation of each image slice acquired during the scan. These may be given by the homogeneous transformation matrix between the image frame and the world coordinate system. The mapping combines the kinematics of the robot (known as a function of joint coordinates) and a constant transformation to the image frame. An estimate of this probe calibration transformation can be obtained from the mechanical design. However, this is not entirely reliable since the geometry of the probes and the placement of the ultrasound transceivers are typically irregular. Therefore, probe calibration was determined experimentally by scanning a planar surface in a water basin, a common ultrasound calibration method [22]. Images were saved in the DICOM format including the pixel spacing (scaling), image position, and image orientation tags. Because the robot may scan in arbitrary directions, special algorithms were developed for 3-D rendering.

VI. EXPERIMENTAL RESULTS AND CLINICAL APPLICATIONS

A. Motion Analysis

An optical tracking system (Polaris, NDI, ON, Canada) was used to measure robot's precision and accuracy. A 6-DoF active marker was mounted in place of the probe, and the axes were commanded independently to positions spanning their limits (within the reading range of the tracker). Each position was repeated ten times. For each static set point, 100 tracker measurements were recorded and averaged. The corresponding joint angles of rotation were calculated based on the 6-DoF measurement. The error for each experiment was determined by the difference between the measured and commanded joint coordinates. Accuracy was calculated as the average of the error data. Precision was determined as difference between the maximum and minimum values. Standard deviation of the errors was also calculated.

Table II shows the experimental values of the measurements. The values in this table, however, should only be trusted up to the level of the measurement instrument capabilities. The stated position accuracy of the Polaris system is on the order of 0.30 mm. But motionless and with averaged readings Polaris measurements may have been better.

B. Robotic Ultrasound Scanning

Several pelvic models were built. Fig. 8(a) shows a mockup simulating the pelvic bones, prostate, bladder, urethra, and two structures representing neurovascular bundles. The body of the mockup and the prostate were made of 300 Bloom gelatin, water, sorbitol, and glycerin (12:100:6:6 by weight). For visual and echogenic delineation, the prostate model also includes brown color flocking (FX Warehouse, Inc., Sarasota, FL) mixed 3% by weight. 2-D images were manually segmented, as usual, and isosurfaces were used for 3-D rendering [see Fig. 8(b)]. Since segmentation is typically slow, volume rendering was also used to display the gathered image space immediately, as shown in Fig. 8(c). Volume rendering displays each gathered image voxel translucent, and light absorption through the voxel is correlated with its brightness according to a scale factor.

TABLE II
POSITIONING PERFORMANCE OF THE TWO ROBOTS

	Experiments	Accuracy	Precision	St. Dev.
3-DoF Robot with Driver R				
θ_1	120	-0.757°	0.059°	0.102°
θ_2	100	-0.227°	0.020°	0.006°
θ_3	80	-0.886°	0.051°	0.015°
4-DoF Robot with Driver RT				
	100	-0.054mm	0.018mm	0.005mm
θ_1	90	-0.361°	0.021°	0.006°
θ_2	90	-0.729°	0.037°	0.012°
θ_3	80	-0.327°	0.147°	0.043°

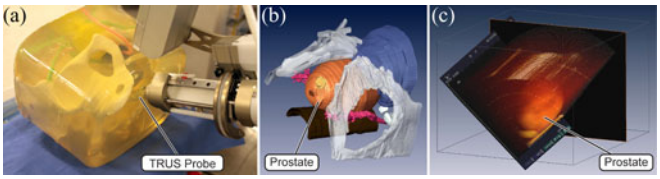

Fig. 8. (a) Pelvic mockup with a TRUS probe supported by the 4-DoF robot, (b) postprocessed 3-D reconstruction from ultrasound images, and (c) 3-D representation of the prostate using volume rendering.

C. Tandem–Robot-Assisted Laparoscopic Radical Prostatectomy (T-RALP)

The first application of the robot has been for assisting the surgeon in radical prostatectomy operations [23]. A precise resection of the tumor-containing prostate gland and the preservation of the neurovascular bundle (NVB) around the prostate are critical in preventing tumor recurrence and preserving sexual potency following radical prostatectomy. However, NVB visualization during surgery can be challenging due to periprostatic connective tissues and intraoperative hemorrhage, even with laparoscopic magnification during RALP with the daVinci robot (Intuitive Surgical, Sunnyvale, CA). A potential solution is image-guided navigation. During RALP there is a limited space between the daVinci surgical robot and the patient, so that a probe cannot be freehanded. Therefore, we used the ultrasound robot to support the probe and perform intraoperative scanning. Fig. 9 shows the schematic setup of the operation. The ultrasound robot is attached to the end of the surgical table, in the confined space below the daVinci robot. As shown in the schematic, ultrasound images are acquired through the robot controller and presented to the surgeon on the console along the current laparoscopic view using a side-by-side display (Tile-Pro).

The Food and Drug Administration has cleared the devices for clinical trial and the Johns Hopkins Institutional Review Board approved the clinical protocol, to evaluate the safety and feasibility of the T-RALP approach. The target goal of T-RALP is to identify and improve the preservation of NVBs around the prostate. Both the 3-DoF and 4-DoF versions have been used clinically. The probe was covered with a standard ultrasound condom and a sterile bag (Easy Equipment Cover, EZ-28, Duckton, TN) pierced over the probe to cover the entire robot and arm. Fig. 10(a) shows the 4-DoF robot covered with the sterile

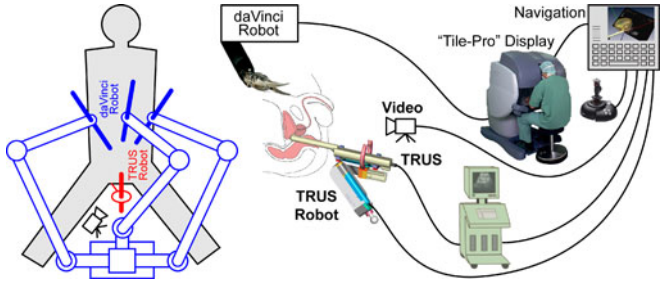

Fig. 9. Schematic setup for T-RALP.

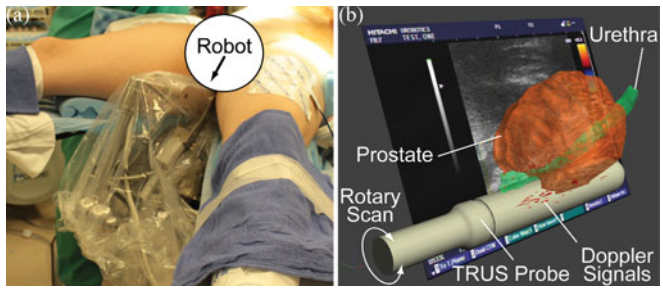

Fig. 10. (a) 4-DoF robot at the beginning of prostatectomy, before docking the daVinci robot and (b) postoperative 3-D reconstruction of pelvic structures based on intraoperative ultrasound scans.

bag supporting an EUP-U533 (Hitachi-Aloka Medical, Twinsburg, OH) wide lateral fire and transversal-type transrectal ultrasound probe (TRUS). This photo is taken before docking the daVinci robot. Images were acquired with an EUS-8500 Digital Ultrasound Scanner (Hitachi-Aloka Medical, Twinsburg, OH) equipped with a wide lateral-fire probe (EUP-U533). Its wide sensor array was able to image the entire prostate with parasagittal views. For the 3-DoF robot this enabled us to image the prostate, with a rotary scan only provided that the probe was properly adjusted manually. Common endocavity probe types include end-fire sagittal, transversal, lateral-fire sagittal, and dual combinations of these types. Whereas the 4-DoF robot has sufficient freedom to handle any of these types, the 3 DoF misses the translation necessary for transversal imaging.

Postoperative segmentation and 3-D reconstruction of the pelvic structures are shown in Fig. 10(b). This includes the prostate, urethra, and Doppler signals of NVBs reconstructed from intraoperative images. Thus far, 46 men underwent T-RALP procedure without associated complications. Median age was 59 years. Each T-RALP portion added approximately 15 min to the surgery. The TRUS probe was controlled remotely. The surgeon was able to observe B-mode and Doppler ultrasound images at critical points of the operation. The 3-DoF robot required a more precise initial setup of the probe so that the prostate was located in the field of view. With the 4-DoF robot, the addition of the insertion motion allowed the probe to be adjusted as needed after the initial setup. With the additional motion transverse images could also be acquired, whereas the 3 DoF could only be used for parasagittal imaging.

VII. Discussion and Conclusion

We report the development of a new medical robot structure for manipulating endocavity ultrasound probes. Its two 3-DoF and 4-DoF versions fall in the middle of the DoF range of other ultrasound robots. For endocavity probes, the 4-DoF robot is kinematically equivalent to human manipulation through an access port or natural orifice. This robot does not restrict the application range of an endocavity probe. We have only performed the T-RALP robot-assisted navigation, but the robot may also be applied to IGI, such as prostate biopsy.

The 3-DoF robot offers advantages in its simplicity. But the application range is also restricted to imaging and certain types of probes (excludes transversal probes) and requires fine DoA prepositioning. Yet its simpler structure makes it usable for external-body probes if the imaging site remains unchanged for the case.

Other robots for endocavity probes have low DoF [9]–[11] because their design requirements focused on needle interventions rather than imaging. At the other end, high-DoF robots were made for external probes [5], [6], [8] being over instrumented for endocavity imaging. The proposed midrange DoF probe manipulators may fill a gap of technology for endocavity ultrasound.

The robots allowed an original surgical approach to prostatectomy, performed on 46 patients thus far. Shortly after our initial clinical report [23], the University of British Columbia group reported that they have also performed a similar procedure on eight patients [11]. Their system presents only 2 DoF, but includes a novel vibratory motion for ultrasound elastography, a great potential for imaging prostate cancer. The T-RALP surgical approach enables the surgeon to observe ultrasound images intraoperatively. Our preliminary data suggest that ultrasound-based navigation is safe and feasible.

References

[1] Logiq-E9 Volume Navigation, GE Healthcare, Waukesha, WI. [Online]. Available: http://www.gehealthcare.com/euen/ultrasound/products/general-imaging/logiq-e9/volume_nav.html

[2] Eigen CA. "Artemis: 3D imaging and navigation for prostate biopsy," [Online]. Available: http://www.eigen.com/products/artemis.cfm

[3] F. Pierrot, E. Dombre, E. Degoulange, L. Urbain, P. Caron, S. Boudet, J. Gariepy, and J. L. Megnien, "Hippocrate: A safe robot arm for medical applications with force feedback," *Med. Image Anal.*, vol. 3, no. 3, pp. 285–300, Sep. 1999.

[4] R. H. Taylor and D. Stoianovici. (2003, Oct.). Medical robotics in computer-integrated surgery. *IEEE Trans. Robot. Autom.* [Online]. 19(5), pp. 765–781. Available: http://urobotics.urology.jhu.edu/pub/2003-taylor-ieeetra.pdf

[5] P. Abolmaesumi, S. E. Salcudean, W. H. Zhu, M. R. Sirouspour, and S. P. DiMaio, "Image-guided control of a robot for medical ultrasound," *IEEE Trans. Robot. Autom.*, vol. 18, no. 1, pp. 11–23, Feb. 2002.

[6] F. Courreges, P. Vieyres, and R. S. Istepanian, "Advances in robotic tele-echography services–The OTELO system," in *Proc. IEEE Eng. Med. Biol. Soc. Conf.*, Sep., 2004, vol. 7, pp. 5371–5374.

[7] C. Delgorge, F. Courreges, L. Al Bassit, C. Novales, C. Rosenberger, N. Smith-Guerin, C. Bru, R. Gilabert, M. Vannoni, G. Poisson, and P. Vieyres, "A tele-operated mobile ultrasound scanner using a light-weight robot," *IEEE Trans. Inf. Technol. Biomed.*, vol. 9, no. 1, pp. 50–58, Mar. 2005.

[8] K. Masuda, Y. Takachi, Y. Urayama, and T. Yoshinaga, "Development of support system to handle ultrasound probe by coordinated motion with medical robot," in *Proc. Annu. Int. Conf. IEEE Eng. Med. Biol. Soc.*, Aug. 2011, vol. 2011, pp. 4519–4522.

[9] H. S. S. Ho, P. Moha, E. D. Lim, D. L. Li, J. S. P. Yuen, W. S. Ng, W. K. O. Lau, and C. W. S. Cheng, "Robotic ultrasound-guided prostate intervention device: System description and results from phantom studies," *Int. J. Med. Robot. Comput. Assist. Surg.*, vol. 5, pp. 51–58, 2009.

[10] H. S. Bassan, R. V. Patel, and M. Moallem, "A novel manipulator for percutaneous needle insertion: Design and experimentation," *IEEE/ASME Trans. Mechatronics*, vol. 14, no. 6, pp. 746–761, Dec. 2009.

[11] T. Adebar, S. Salcudean, S. Mahdavi, M. Moradi, C. Nguan, and L. Goldenberg, "A robotic system for intra-operative trans-rectal ultrasound and ultrasound elastography in radical prostatectomy," in *Proc. 2nd Int. Conf. Inf. Process. Comput.-Assist. Intervent.*, pp. 79–89, 2011.

[12] V. Mallapragada, N. Sarkar, and T. K. Podder, "Toward a robot-assisted breast intervention system," *IEEE/ASME Trans. Mechatronics*, vol. 16, no. 6, pp. 1011–1020, Dec. 2011.

[13] B. Eldridge, K. Gruben, D. LaRose, J. Funda, S. Gomory, J. Karidis, G. McVicker, R. Taylor, and J. Anderson, "A remote center of motion robotic arm for computer assisted surgery," *Robotica*, vol. 14, pp. 103–109, Jan./Feb. 1996.

[14] M. Piccigallo, U. Scarfogliero, C. Quaglia, G. Petroni, P. Valdastri, A. Menciassi, and P. Dario, "Design of a novel bimanual robotic system for single-port laparoscopy," *IEEE/ASME Trans. Mechatronics*, vol. 15, no. 6, pp. 871–878, Dec. 2010.

[15] D. Stoianovici, B. E. Paden, P. Mozer, K. Masamune, and R. L. Galloway, "Guest editorial introduction to the focused section on surgical and interventional medical devices," *IEEE/ASME Trans. Mechatronics*, vol. 15, no. 6, pp. 829–837, Dec. 2010.

[16] G. Zong, X. Pei, J. Yu, and S. Bi, "Classification and type synthesis of 1-DOF remote center of motion mechanisms," *Mech. Mach. Theory*, vol. 43, no. 12, pp. 1585–1595, Dec. 2008.

[17] J. A. Cadeddu, D. Stoianovici, R. N. Chen, R. G. Moore, and L. R. Kavoussi. (1998, Apr.). Stereotactic mechanical percutaneous renal access. *J. Endourol.* [Online]. *12(2)*, pp. 121–125. Available: http://urobotics.urology.jhu.edu/pub/1998-cadeddu-endourology.pdf

[18] D. Stoianovici, L. L. Whitcomb, J. H. Anderson, R. H. Taylor, and L. R. Kavoussi. (1998). "A modular surgical robotic system for image guided percutaneous procedures," in *MICCAI* (Lecture Notes in Computer Science 1496) [Online]. pp. 404–410. Available: http://urobotics.urology.jhu.edu/pub/1998-stoianovici-miccai.pdf

[19] D. Stoianovici, L. Whitcomb, D. Mazilu, R. Taylor, and L. Kavoussi. (2006, Apr. 4). "Remote center of motion robotic system and method," U.S. Patent 07021173 (C03980) [Online]. Available: http://urobotics.urology.jhu.edu/pub/2006-stoianovici-uspto-07021173.pdf

[20] D. Stoianovici and L. Kavoussi. (2006, May 30). "Ball-worm transmission," U.S. Patent 7051610 (C03512) [Online]. Available: http://urobotics.urology.jhu.edu/pub/2006-stoianovici-uspto-07051610.pdf

[21] D. Stoianovici K. Cleary, A. Patriciu, D. Mazilu, A. Stanimir, N. Craciunoiu, V. Watson, and L. R. Kavoussi. (2003, Oct.). AcuBot: A robot for radiological interventions. *IEEE Trans. Robot. Autom.* [Online]. *19(5)*, pp. 926–930. Available: http://urobotics.urology.jhu.edu/pub/2003-stoianovici-ieeetra.pdf

[22] R. W. Prager, R. N. Rohling, A. H. Gee, and L. Berman, "Rapid calibration for 3-D freehand ultrasound," *Ultrasound Med. Biol.*, vol. 24, no. 6, pp. 855–869, Jul. 1998.

[23] M. Han, C. Kim, P. Mozer, F. Schafer, S. Badaan, B. Vigaru, K. Tseng, D. Petrisor, B. Trock, and D. Stoianovici. (2011, Feb.). Tandem-robot assisted laparoscopic radical prostatectomy to improve the neurovascular bundle visualization: A feasibility study. *Urology*, [Online]. *77(2)*, pp. 502–506. Available: http://urobotics.urology.jhu.edu/pub/2011-han-urology.pdf

Dan Stoianovici received the Ph.D. degree from Southern Methodist University, Dallas, TX, in 1996.

He is a Professor of Urology, Mechanical Engineering, and Neurosurgery at The Johns Hopkins University, Baltimore, MD. He is also the Director of the Urology Robotics Program. His specialty is medical robotics, in particular, robotic hardware. His research interests include design, manufacturing, and control of robots for direct image-guided intervention. He is the author of numerous articles, presentations, and 12 issued patents of invention.

Dr. Stoianovici received the 2008 Best Paper Award of the IEEE/ASME TRANSACTIONS ON MECHATRONICS. He is a Section Editor for the *Journal of Endourology*, the Executive Director of the Engineering and Urology Society, an Associate Editor for *International Journal of Medical Robotics and Computer Aided Surgery*, a member of the Editorial Board for *Minimally Invasive Therapy and Allied Technologies*, and a Technical Editor for the IEEE/ASME TRANSACTIONS ON MECHATRONICS. He serves on National Institutes of Health study sections and other grant foundations. He is also a member of the ASME.

Chunwoo Kim (S'10) received the B.S. degree from the Department of Mechanical Aerospace Engineering, Seoul National University, Seoul, Korea, in 2008. He is currently working toward the Ph.D. degree in mechanical engineering at The Johns Hopkins University, Baltimore, MD.

Since 2008, he has been a Researcher in the Urology Robotics Laboratory, The Johns Hopkins University. His research interests include the control of medical image-guided robots.

Dr. Kim is a recipient of the Fulbright scholarship and the Prostate Cancer Research Training Award of the United States Department of Defense.

Felix Schäfer received the M.S. degree in mechanical engineering and economics from the University of Paderborn, Paderborn, Germany, and the Ph.D. degree from the University of Genova, Genova, Italy, in 2006 and 2010, respectively.

He joined the Urology Robotics research group at The Johns Hopkins University as an exchange student in 2009. He is with TWT GmbH Science and Innovation, Neuhausen, Germany. His specialty is the design of interventional and surgical robots. He is the author of several articles and holds one patent of invention.

Chien-Ming Huang received the M.D. degree from the Medicine Department of the National Defense Medical Center, Taipei, Taiwan, in 1995. He also received the Master of Arts degree from the Graduate Institute of Religious and Cultural Studies, Tzu Chi University, Hualien, Taiwan.

He is a Board-Certified Urologist practicing in Taiwan. He has completed medical center multidisciplinary surgical training and is a specialist in general surgery and urology. He is also the Chairman of the Division of Urology, Department of Surgery, Hualian Armed Forces General Hospital. His specialty is urologic laparoscopic surgery and stone treatment. His research interests include image diagnosis and endoscopic surgery. He is the author of numerous articles and presentations.

Yihe Zuo received the Bachelor's degree from An-Hui University of Science and Technology, Anhui, China, in 2002. He is currently working toward the Ph.D. degree at Beijing Institute of Technology, Beijing, China.

He is currently an Electrocardiogram Intelligent Diagnosis System Engineer at Beijing Safe Heart Technology Ltd, Beijing. Between 2010 and 2012, he was an exchange Ph.D. student at The Johns Hopkins University. His interests include image-guided intervention medical robots development, medical image processing, and 3-D visualization. He was also involved in research on hybrid electrical vehicles energy management and control strategies, vehicle transmission, and electrical control system design.

Doru Petrisor received the M.S. degree in mechanical engineering from the University of Craiova, Craiova, Romania, in 1988, and the Ph.D. degree from the University of Petrosani, Petrosani, Romania, in 2002, followed by a research fellowship in urology at The Johns Hopkins University.

Between 1991and 1994, he was Assistant Professor at the University of Craiova, where he became a Lecturer. In 2002, he joined the Urology Robotics research group at The Johns Hopkins University, Baltimore, MD, where he is currently a Research Associate Professor. He specializes in design of interventional and surgical robots, medical instrumentation, and CNC manufacturing. He is the author of numerous articles, presentations, and four patents of invention.

Dr. Petrisor is a member of the ASME.

Misop Han received the M.D. degree from the School of Medicine, The Johns Hopkins University, Baltimore, MD, and the M.S. degree from Feinberg School of Medicine, Northwestern University, Chicago, IL.

He is an Associate Professor of Urology and Oncology at the James Buchanan Brady Urological Institute, Johns Hopkins Medicine. His main clinical focus is on urological oncology with a special emphasis on prostate cancer and kidney cancer. His research interests include the outcome of radical prostatectomy and image-guided surgery using surgical robots. He has published extensively on these subjects.